NATIONAL ADVISORY COMMITTEE
FOR AERONAUTICS

TECHNICAL NOTE

No. 1295

WIND-TUNNEL INVESTIGATION OF THE AIR LOAD DISTRIBUTION

ON TWO COMBINATIONS OF LIFTING SURFACE AND FUSELAGE

By Carl A. Sandahl and Samuel D. Vollo

Langley Memorial Aeronautical Laboratory
Langley Field, Va.

Washington
May 1947

NATIONAL ADVISORY COMMITTEE FOR AERONAUTICS

TECHNICAL NOTE NO. 1295

WIND-TUNNEL INVESTIGATION OF THE AIR LOAD DISTRIBUTION

ON TWO COMBINATIONS OF LIFTING SURFACE AND FUSELAGE

By Carl A. Sandahl and Samuel D. Vollo

SUMMARY

Wind-tunnel measurements have been made of the air load
distribution on a canard-type model. Two combinations of
lifting surface and fuselage, representing appreciable variation
of lifting-surface span relative to fuselage diameter, were
obtained by removing separately the wing and stabilizer of the
model. The tests also included measurements of lift, drag,
and pitching moment for several configurations. The results
show that, for the configurations tested, the spanwise loadings
on the combinations agreed fairly well with the loadings calcu-
lated by Lennertz's method.

INTRODUCTION

A theoretical approach to the problem of lifting-surface-
fuselage interference is given in reference 1 in which the span-
wise loading is obtained for a lifting line intersecting the
center line of an infinitely long circular cylinder. This
analysis predicts a decrease in the spanwise loading over the
fuselage and a reduction in total lift as compared with the
spanwise loading and lift of the wing alone at the same angle of
attack. Measurements of the lift of a large number of wing-
fuselage combinations (reference 2) indicate, however, that
the lift of the wing-fuselage combination is more nearly equal
to the lift of the wing alone. Over-all lift measurements of
wings and wing-fuselage combinations, however, do not define
the spanwise load curve. The purpose of the present investigation
is to present data relating to the measured and calculated span-
wise loadings on two combinations of lifting surface and fuselage
having appreciable variation of span relative to fuselage diameter.
The tests included measurements of pressure distribution, lift,
drag, and pitching moment for several model configurations over
a range of angles of attack at several yaw angles.

SYMBOLS

P pressure coefficient $\left(\dfrac{p - p_0}{q_0}\right)$

$\dfrac{d(N/q_0)}{dy}$ section load derivative for horizontal surfaces

C_N normal-force coefficient $(N/q_0 S)$

C_L lift coefficient $(L/q_0 S)$

C_D total drag coefficient $(D/q_0 S)$

C_{D_0} profile-drag coefficient $(D_0/q_0 S)$

C_{D_S} drag coefficient based on stabilizer area $(D/q_0 S_S)$

C_{L_S} lift coefficient based on stabilizer area $(L/q_0 S_S)$

C_m pitching-moment coefficient $(M/q_0 \bar{S} \bar{c})$

p local static pressure

p_0 free-stream static pressure

q_0 free-stream dynamic pressure

N normal force

L lift

D total drag

D_0 profile drag

S wing area (19.86 sq ft)

S_S stabilizer area (4.06 sq ft)

$\bar{c}$ wing mean aerodynamic chord (1.87 ft)

c local wing chord

b wing span (11.00 ft)

b_S stabilizer span (4.62 ft)

A   aspect ratio

l · fuselage length (15.98 ft)

α angle of attack, degrees

ψ angle of yaw, positive when nose is displaced to
             right, degrees

ϕ angular position of generatrix of fuselage body of
             revolution, measured from the vertical plane of
             symmetry, degrees

d fuselage diameter at quarter chord of wing

d_s fuselage diameter at quarter chord of stabilizer

x longitudinal coordinate parallel to fuselage center
             line

y lateral coordinate perpendicular to plane of symmetry

z vertical coordinate perpendicular to x,y plane

APPARATUS AND TESTS

The test model used was constructed of plywood and was
finished to a fair aerodynamic surface. The general arrange-
ment of the model is shown in figure 1. The wing, stabilizer,
and vertical tail were removable from the fuselage, which was
a body of revolution. All control surfaces were set at neutral
and the gaps were sealed for this investigation.

The model was mounted in the Langley propeller-research
tunnel on the six-component-balance system as shown in figure 2.
The model was attached at the center of gravity to a single
support strut by means of a universal fitting which permitted
the setting of pitch and yaw angles. Motion in pitch was
restrained by a "nose" wire, the lower end of which was attached
to a balance to allow the measurement of pitching moments. The
tunnel balance system was used to measure lift and drag.

The pressure distribution on the fuselage was obtained by
orifices flush with the surface and arranged as shown in figure 1.
Chordwise pressure distributions on the right wing panel and the

left stabilizer panel were measured by means of pressure belts.
On the basis of the results reported in references 3 and 4, the
belt method of pressure-distribution measurement is considered
to be of sufficient accuracy for the present investigation.

The investigation consisted of measurements of lift, drag,
pitching moment, and pressure distributions over a range of
angles of attack from -2° to 16° and at angles of yaw of ±10°,
±5°, and 0°. The unsymmetric distribution of fuselage orifices
necessitated tests at equal positive and negative angles of yaw
in order to obtain complete fuselage pressure distributions.
At zero yaw, the pressures at points at equal angular displace-
ment from the vertical plane of symmetry are considered to be
equal. The following configurations were tested and are desig-
nated herein as follows:

Configuration	Designation
Fuselage with wing, stabilizer, and vertical tail	FWST
Fuselage with wing and vertical tail	FWT
Fuselage with wing	FW
Fuselage with stabilizer and vertical tail	FST
Fuselage alone	F

The test velocity was varied from 80 to 100 miles per hour
corresponding to a Reynolds number range from 1.4 to 1.7 × 10⁶
based on the wing mean aerodynamic chord of 1.87 feet.

RESULTS

The results are presented in figures 3 to 10. Corrections
for jet-boundary effects have been applied to the angle of attack
and the drag coefficient. The tare drag was estimated and has
been applied to the measured drag.

The fuselage pressure distribution for different angles of
attack and yaw for configurations F and FWST are shown in
figures 3 to 5. The pressure distributions for the various
positions of the generatrix of the fuselage were obtained by

cross-plotting the pressure distributions measured at the various
longitudinal stations of the fuselage. The pressure distributions
in the plane of symmetry for configurations F, FST, and FW are
given in figure 6.

The spanwise loading curves for the wing and stabilizer
are given in figures 7 and 8. Outboard of the fuselage the
section load derivative $\dfrac{d(N/q_o)}{dy}$ was obtained by integrating
chordwise pressure distributions measured at three stations along
the semispans of the wing and stabilizer. The fuselage section
loadings induced by the wing were obtained by superimposing
fuselage pressure-distribution curves for configurations F
and FW drawn for the vertical plane of symmetry and for a
parallel plane displaced 5 inches. The total difference in the
areas of the pressure diagrams for the two configurations was
then used in computing the section load derivative $\dfrac{d(N/q_o)}{dy}$. An
identical procedure utilizing configurations F and FST was
used in computing the load induced on the fuselage by the
stabilizer.

The variation of lift, drag, and pitching-moment coefficients
with angle of attack for several configurations is shown in
figure 9. Measurements for configuration FST at $\psi = 0^o$ are
not available; the curves for this configuration were obtained
by extrapolating tests at $\psi = \pm 5^o$ and $\pm 10^o$. The coefficients
are based on wing dimensions regardless of configuration.

DISCUSSION

Fuselage pressure distribution.- Although isolation of the
effects of the individual components is not possible, the general
manner in which the lifting surfaces affect the distribution of
pressure on the fuselage is shown in figures 3 to 5. In general,
the main effects of the wing or stabilizer are limited to the
immediate vicinity of the fuselage junctures of the wing and
stabilizer. The distance along the fuselage over which the
fuselage pressure distribution is materially affected by either
the wing or stabilizer is shown more clearly in figure 6 to be
approximately a distance of one chord ahead of the leading edge
and one chord behind the trailing edge of each of the components.
Defining these limits is difficult, inasmuch as the pressure-
distribution curves for the different configurations are asymptotic.

Spanwise loadings.- The measured and calculated spanwise
load distributions are shown in figures 7 and 8. The spanwise
load distributions predicted by the theory (reference 1) are in
agreement with the measured spanwise load distributions. The
agreement was particularly good for the configuration FST,
for which the conditions assumed in deriving the theory were
more nearly fulfilled. In deriving the theory, the fuselage
is assumed to be infinite in length and at zero angle of attack,
the wing axis and fuselage axis are assumed to intersect, and
the loading is considered to be such that the induced drag is
a minimum. In addition, the wing chord should be comparatively
small with respect to the span and the fuselage diameter should
not be small in comparison with the wing chord. It has been
suggested from theoretical considerations that the loss in load
over the lifting-surface in the vicinity of the fuselage would
be regained on the fuselage, where it is tapered to finite length;
however, no such increase in load over the rear of the fuselage
was measured in these tests, probably because of fuselage boundary-
layer effects. Evidence of appreciable fuselage boundary layer
is indicated by the pressure-distribution curves of configuration F
(fig. 6(a)), which show that almost no negative lift is developed
over the rear of the fuselage. This lack of negative lift over
the rear of the fuselage probably accounts, in part, for the lack
of agreement between the calculated and measured pitching-moment
coefficients of figure 9. The calculated pitching-moment coef-
ficients in this figure for configuration F were made by the
method of reference 5.

Induced drag.- The induced-drag coefficients associated with
the measured spanwise loadings on the wing and stabilizer were
computed by the method of reference 6 and are shown in figure 10.
Substantially the same induced-drag coefficients were obtained
from a 6-point and a 10-point Fourier series determination; thus,
a sufficient number of points were indicated to have been utilized
in the analysis.

A comparison (fig. 10(a)) of the induced-drag coefficient
computed from the measured spanwise loadings on the wing-fuselage
combination and the minimum induced-drag coefficient for the
combination computed from the method of reference 1 indicates
a reduction in effective aspect ratio of 19 percent as a result
of distortion of the measured spanwise load distribution from
the ideal load distribution for the combination. Good agreement
exists between the induced-drag coefficient obtained from the
force tests and from the measured spanwise loadings.

A similar comparison (fig. 10(b)) for the stabilizer-
fuselage combination indicates exact agreement between the

induced-drag coefficient computed from the measured spanwise loadings and computed from reference 1. The exact agreement for this configuration results from the good agreement between the measured and calculated spanwise load distributions.

## CONCLUSIONS

Results of an experimental investigation to determine the spanwise loading for several combinations of fuselage and lifting surface showed reasonable agreement between the measured loadings and the calculated loadings obtained by Lennertz's method.

Langley Memorial Aeronautical Laboratory
    National Advisory Committee for Aeronautics
        Langley Field, Va., February 19, 1947

REFERENCES

1. Lennertz, J.: Influence of the Airplane Body on the Wings.
      Vol. IV of Aerodynamic Theory, div. K, ch. III, sec. 1,
      W. F. Durand, ed., Julius Springer (Berlin), 1935, pp. 152-157.

2. Jacobs, Eastman N., and Ward, Kenneth E.: Interference of
      Wing and Fuselage from Tests of 209 Combinations in the
      N.A.C.A. Variable-Density Tunnel. NACA Rep. No. 540, 1935.

3. Corson, Blake W., Jr.: The Belt Method for Measuring Pressure
      Distribution. NACA RB, Feb. 1943.

4. Zalovcik, John A., and Daum, Fred L.: Flight Investigation at
      High Mach Numbers of Several Methods of Measuring Static
      Pressure on an Airplane Wing. NACA RB No. L4H10a, 1944.

5. Munk, Max M.: The Aerodynamic Forces on Airship Hulls.
      NACA Rep. No. 184, 1924.

6. Glauert, H.: The Elements of Aerofoil and Airscrew Theory.
      Cambridge Univ. Press, 1926, pp. 139-140.

Fig. 1

Letters denote stations at which fuselage orifices are located.

152.0

Location of pressure distribution belts

C/4

13.7

39.6

59.3

Stations P to T

Stations H to 0

55.5

C/2

Location of pressure distribution belts

Stations A to 4

10.0

18.1

25.0

Distribution of fuselage orifices
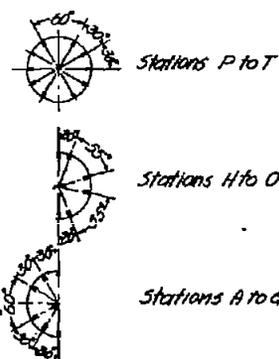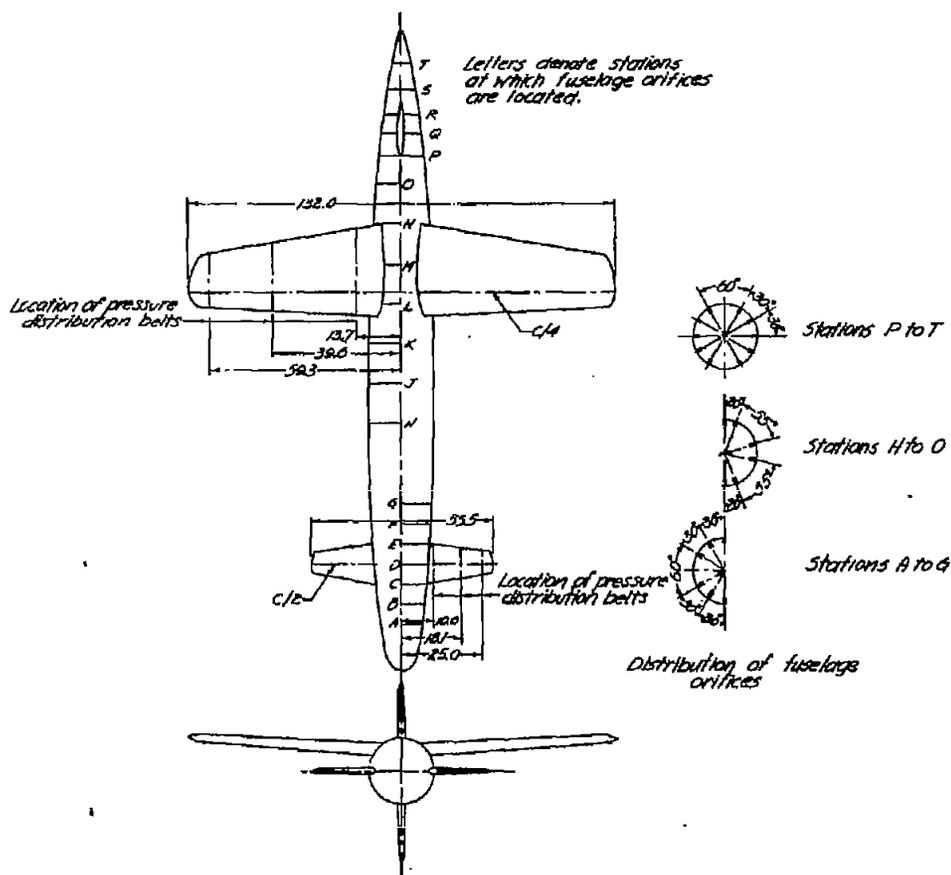
Wing

| Airfoil (root to tip)	NACA 66,2-016
Tip chord, in.	14.40
Root chord, in.	31.10
Area, sq ft	19.86
Geometric twist, deg	0
Aspect ratio	6.09
Incidence, deg	1.0
Dihedral, deg	4.0
M.A.C.	22.4

Stabilizer

Airfoil (root to tip)	NACA 66,2-012
Tip chord, in.	6.00
Root chord, in.	19.32
Area, sq ft	4.06
Geometric twist, deg	0
Aspect ratio	5.27
Incidence, deg	-0.7
Dihedral, deg	0.

Vertical tail

Airfoil (root to tip)	66,2-015
Tip chord	7.94
Root chord (5.75" from ₵)	18.40
Area, sq ft	4.90
Aspect ratio	4.05

Dimensions of all aerodynamic surfaces obtained by extending the leading and trailing edges to plane of symmetry

C

.08c

.10c

.20c

.35c

.55c

.75c

.95c
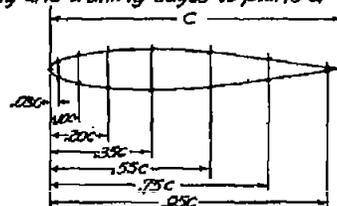
Chordwise distribution of orifices for all pressure distribution belts

191.8

161.7

113.1

96.0

32.9

C/2 of stabilizer

C/4 of wing

53.6

Pitching-moment axis

4.75 R

20.00 (max. diam)

C/2 of vertical tail

$\frac{Local\ diameter}{Maximum\ diameter}$

1.0
.8
.6
.4
.2
0

0 .1 .2 .3 .4 .5 .6 .7 .8 .9 1.0

Relative distance from nose, x/l

NATIONAL ADVISORY
COMMITTEE FOR AERONAUTICS

Fuselage thickness distribution
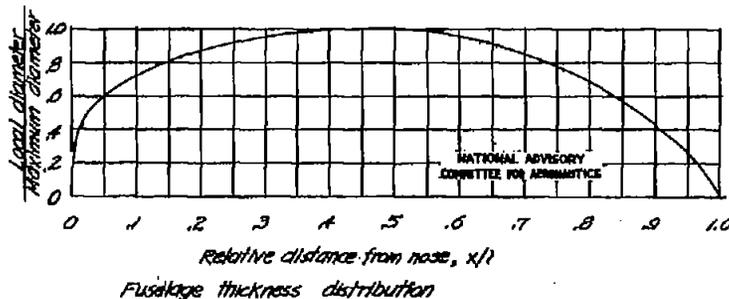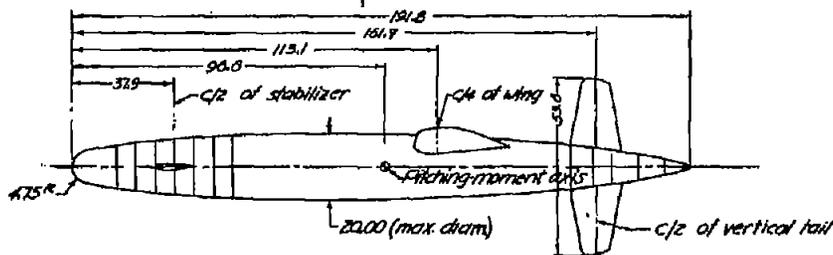
Figure 1.- Geometric details of model.
(All dimensions not specified are in inches.)
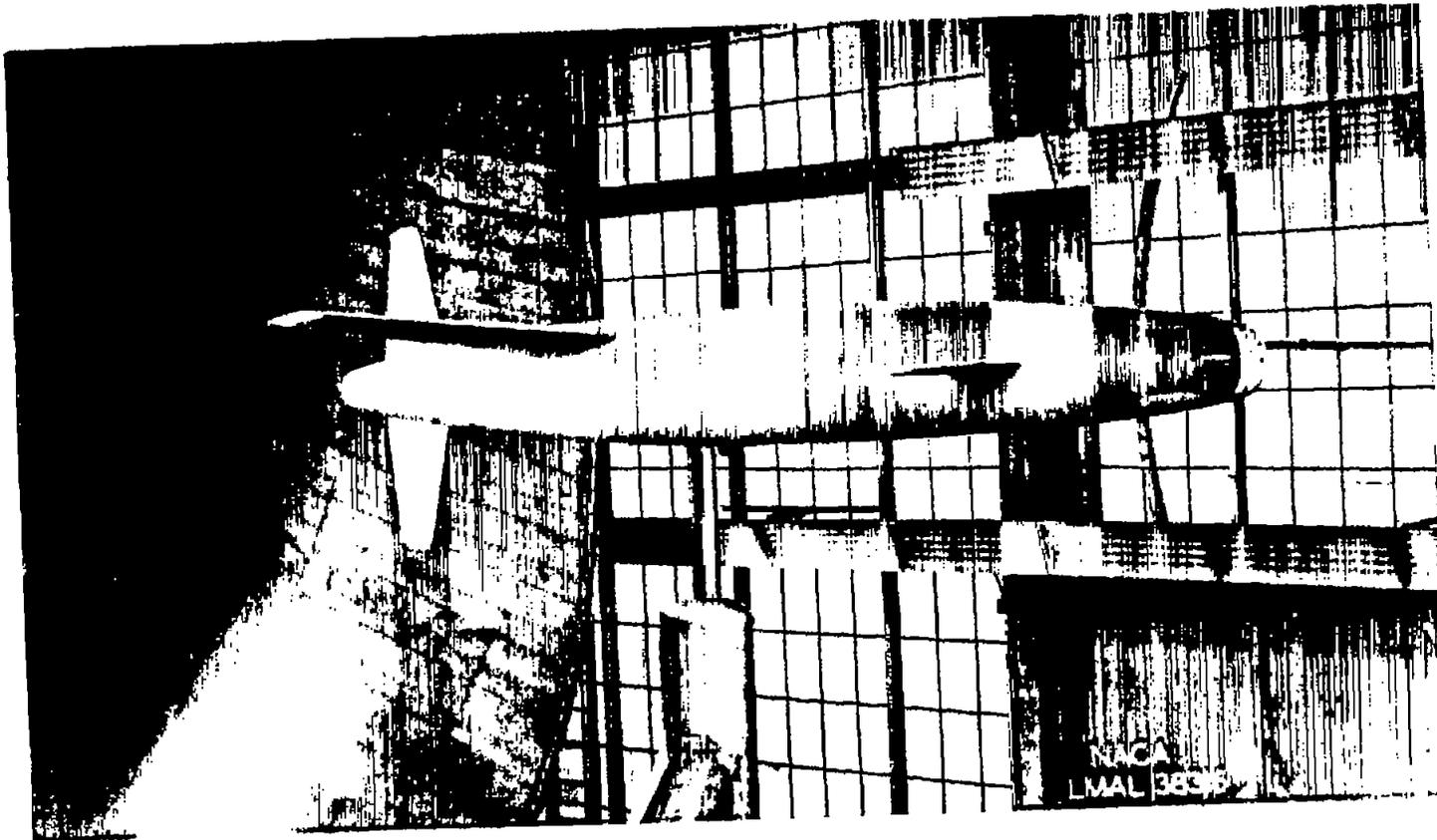
(a) Configuration FWST.

Figure 2.- Model installed for testing.

NACA
LMAL 44489
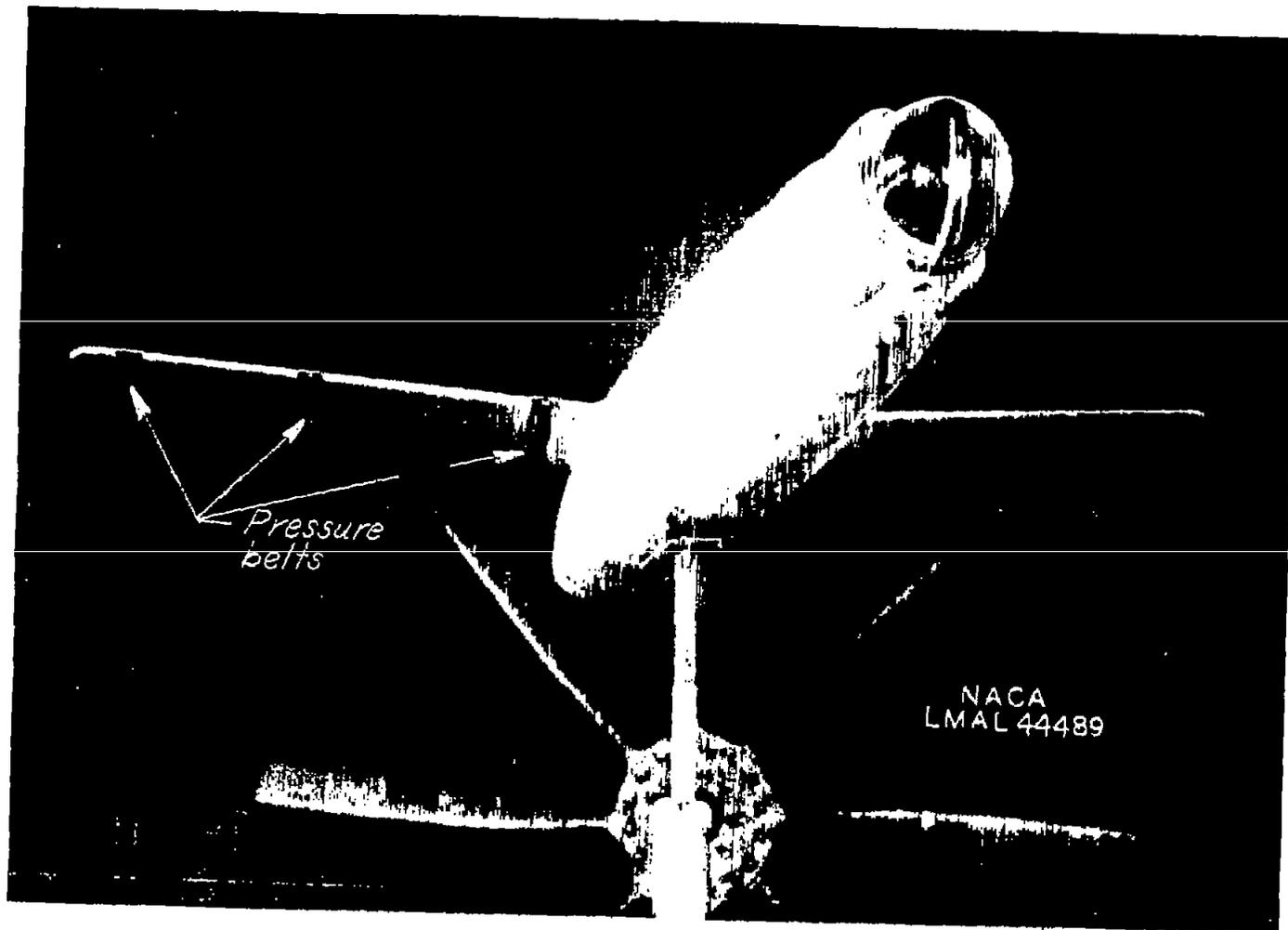
(b) Configuration FW.

Figure 2.- Concluded.

(a) Configuration F.

(b) Configuration FWST.
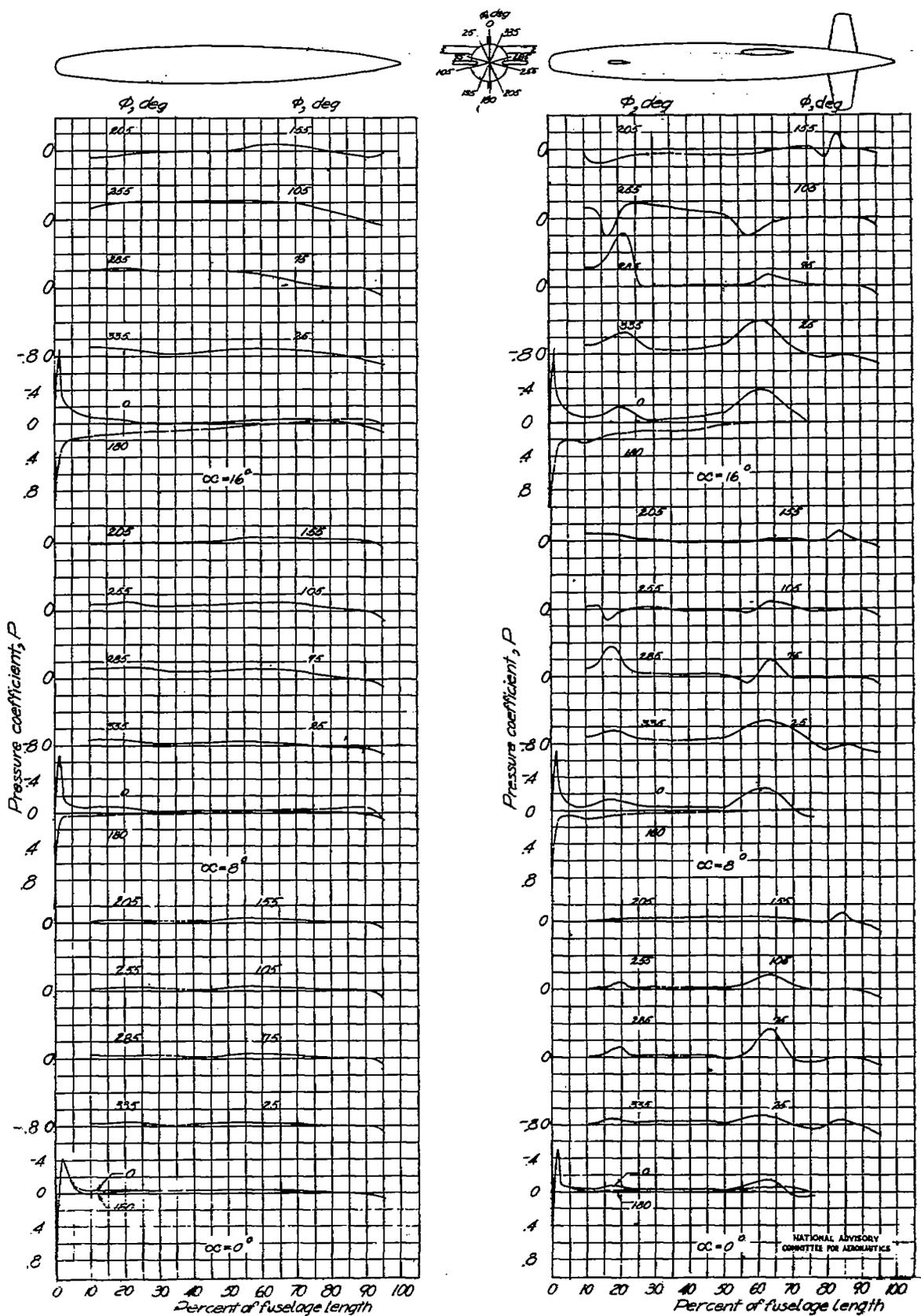
Figure 3.- Fuselage pressure distribution for several positions of the generatrix. ψ = 0°.

Fig. 4   NACA TN No. 1295
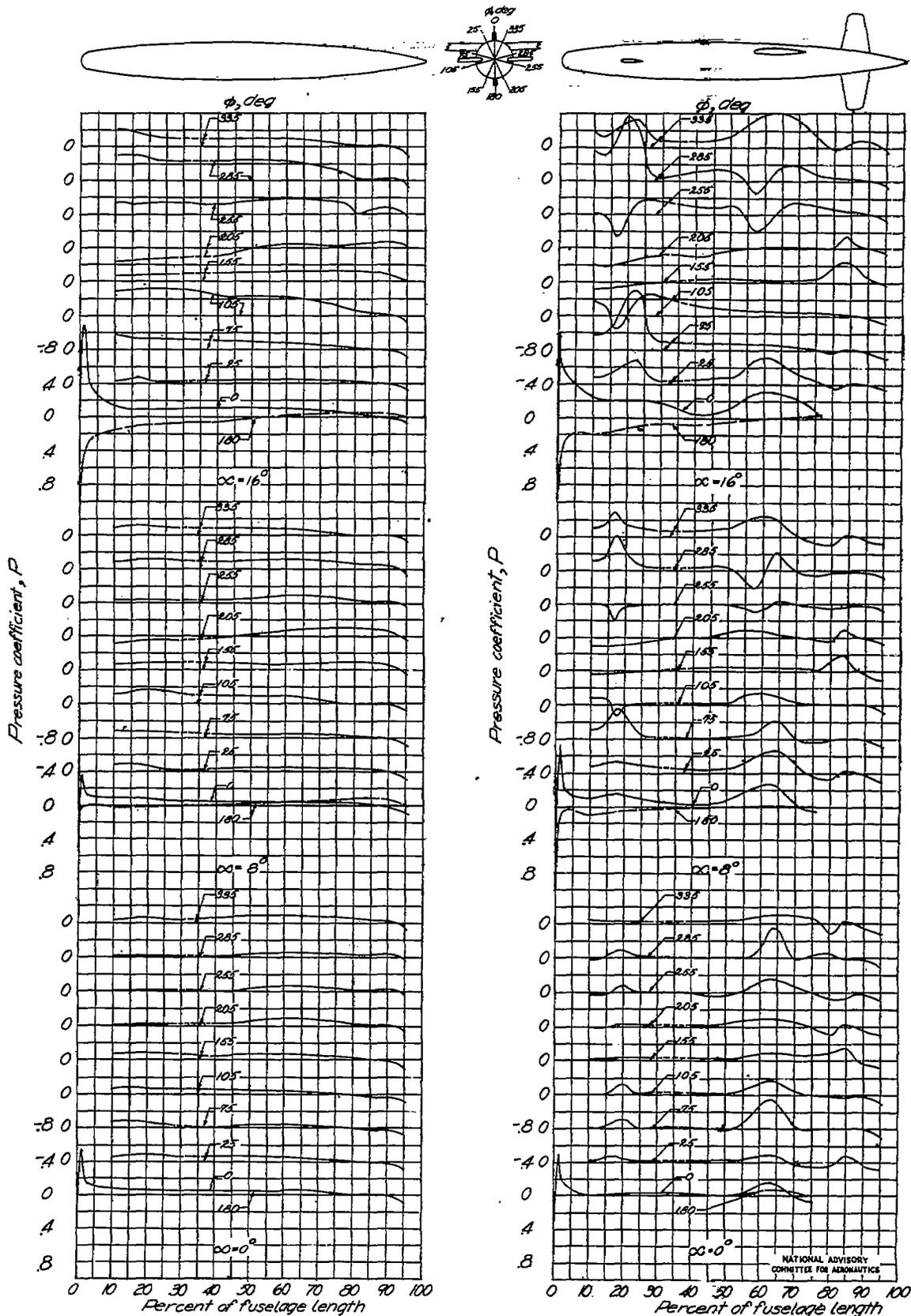
Figure 4.- Fuselage pressure distribution for several positions of the generatrix. $\psi = 5°$.

(a) Configuration F.

(b) Configuration FWST.
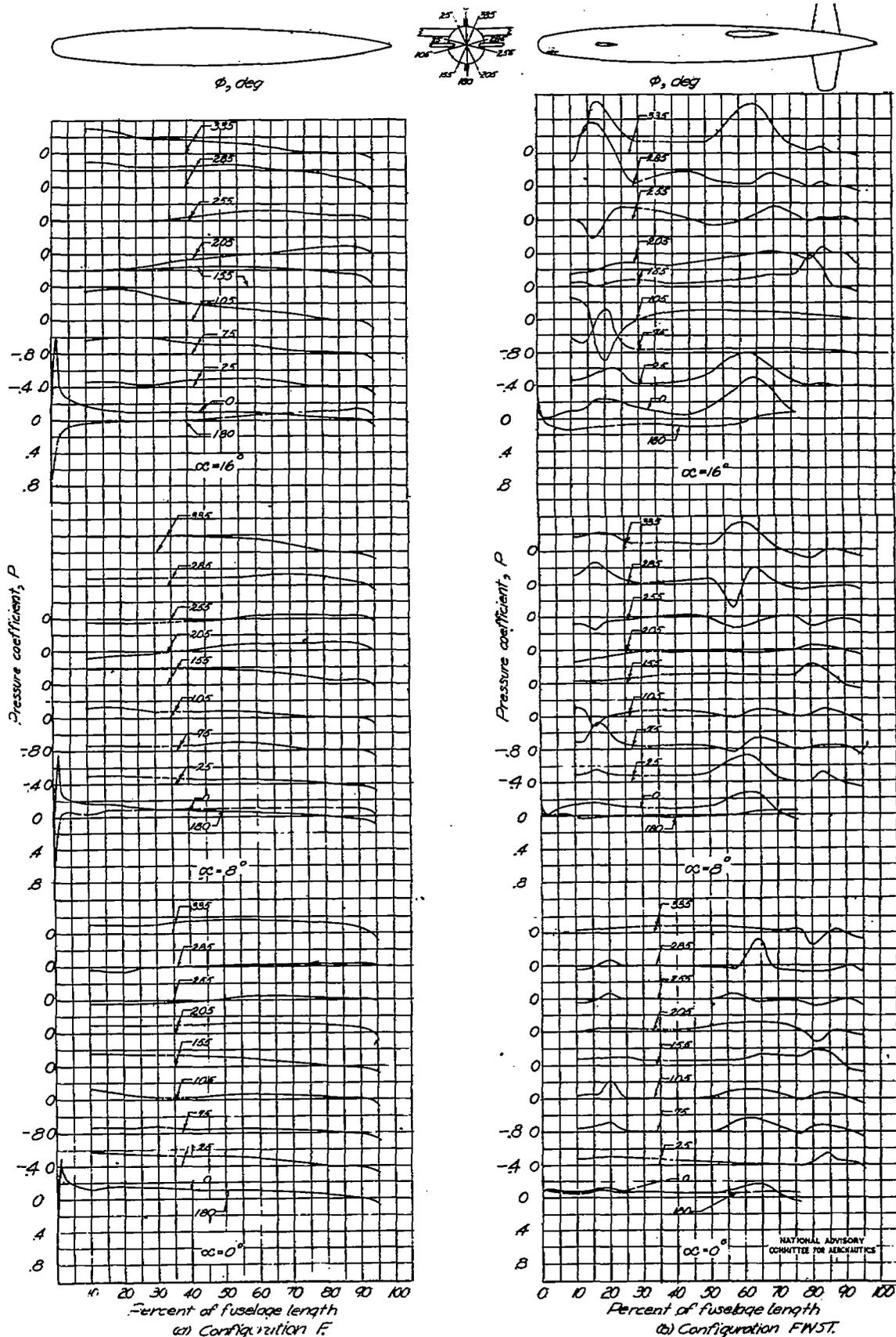
Figure 5.- Fuselage pressure distribution for several positions of the generatrix. φ = 10°.

(a) Configuration F.

(b) Configuration FWST.

Percent of fuselage length

Pressure coefficient, P

φ, deg

Fig. 6

Figure 6 .- Effect of stabilizer and wing on fuselage pressure distribution for plane of symmetry. $\psi = 0°$.
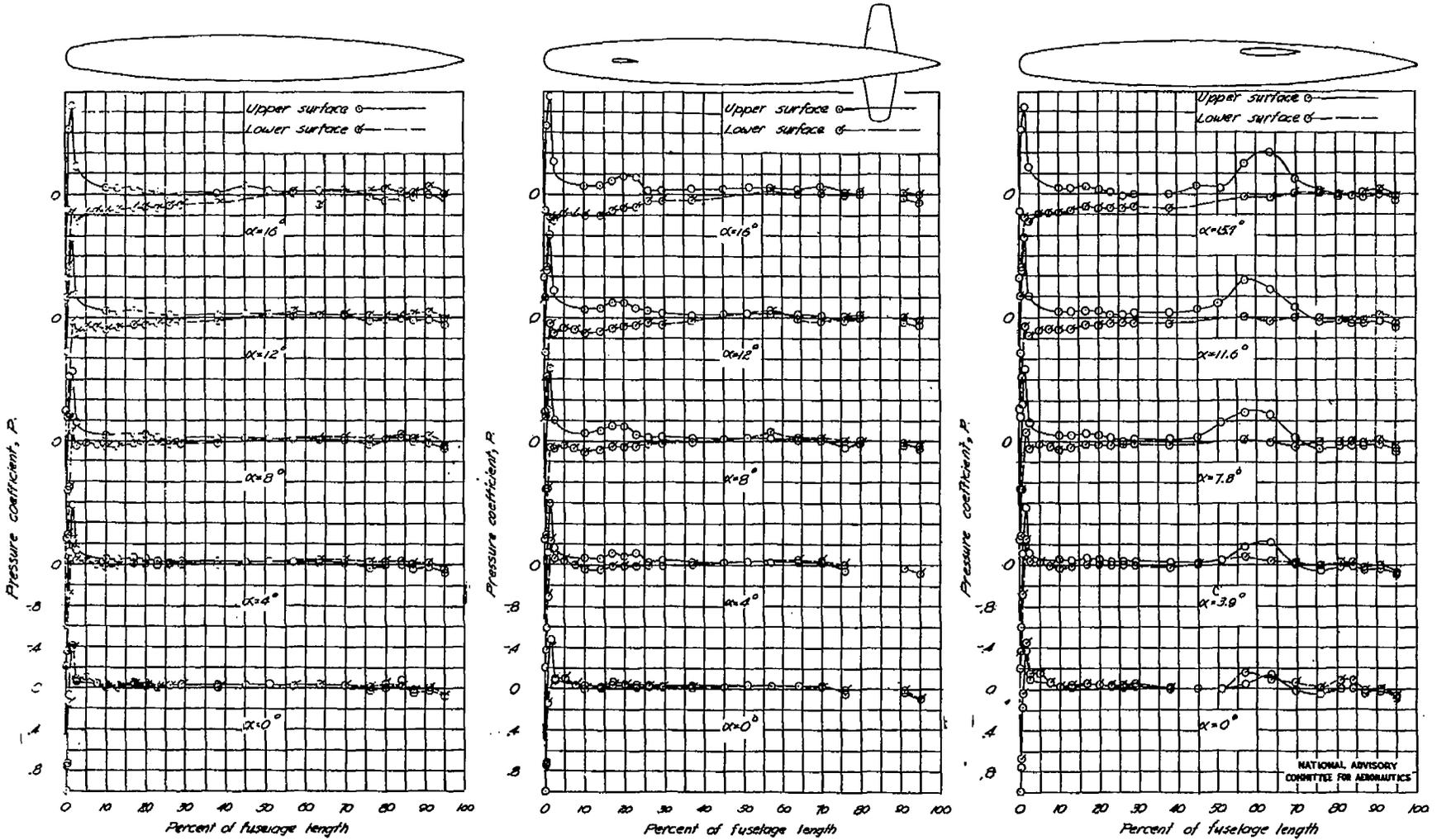
(a) Configuration F.

(b) Configuration FST.

(C) Configuration FW.

Percent of fuselage length

Percent of fuselage length

Percent of fuselage length

Pressure coefficient, P

Pressure coefficient, P

Pressure coefficient, P

Upper surface
Lower surface

Upper surface
Lower surface

Upper surface
Lower surface

$\alpha = 16°$

$\alpha = 12°$

$\alpha = 8°$

$\alpha = 4°$

$\alpha = 0°$

$\alpha = 16°$

$\alpha = 12°$

$\alpha = 8°$

$\alpha = 4°$

$\alpha = 0°$

$\alpha = 15.7°$

$\alpha = 11.6°$

$\alpha = 7.8°$

$\alpha = 3.9°$

$\alpha = 0°$

NATIONAL ADVISORY
COMMITTEE FOR AERONAUTICS

Figure 7 .— Comparison of theoretical and experimental wing span loading. $\psi = 0°$; configuration FWT.

Fig. 8   NACA TN No. 1295
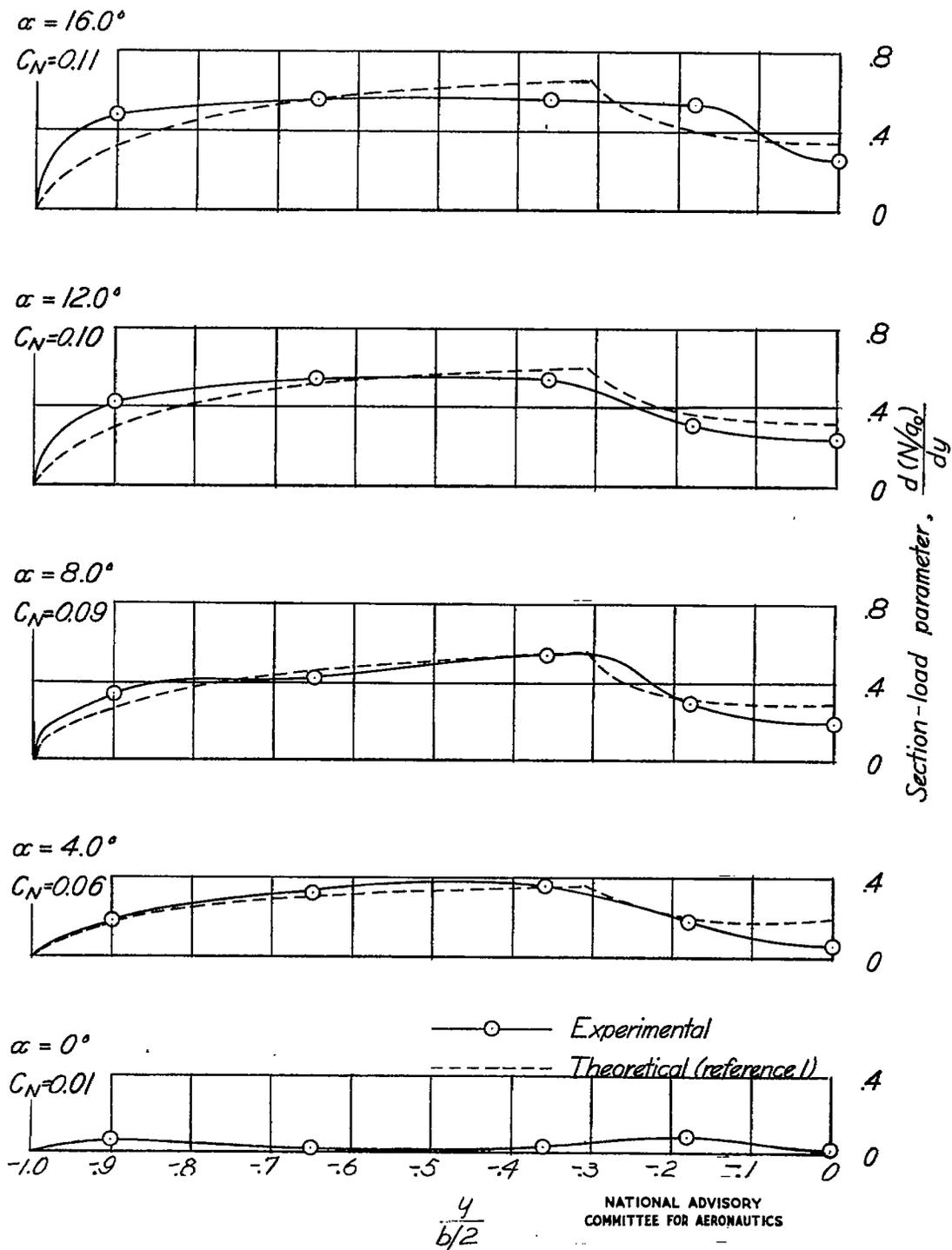
Figure 8.— Comparison of theoretical and experimental stabilizer span loading. $\psi=0°$; configuration FST.
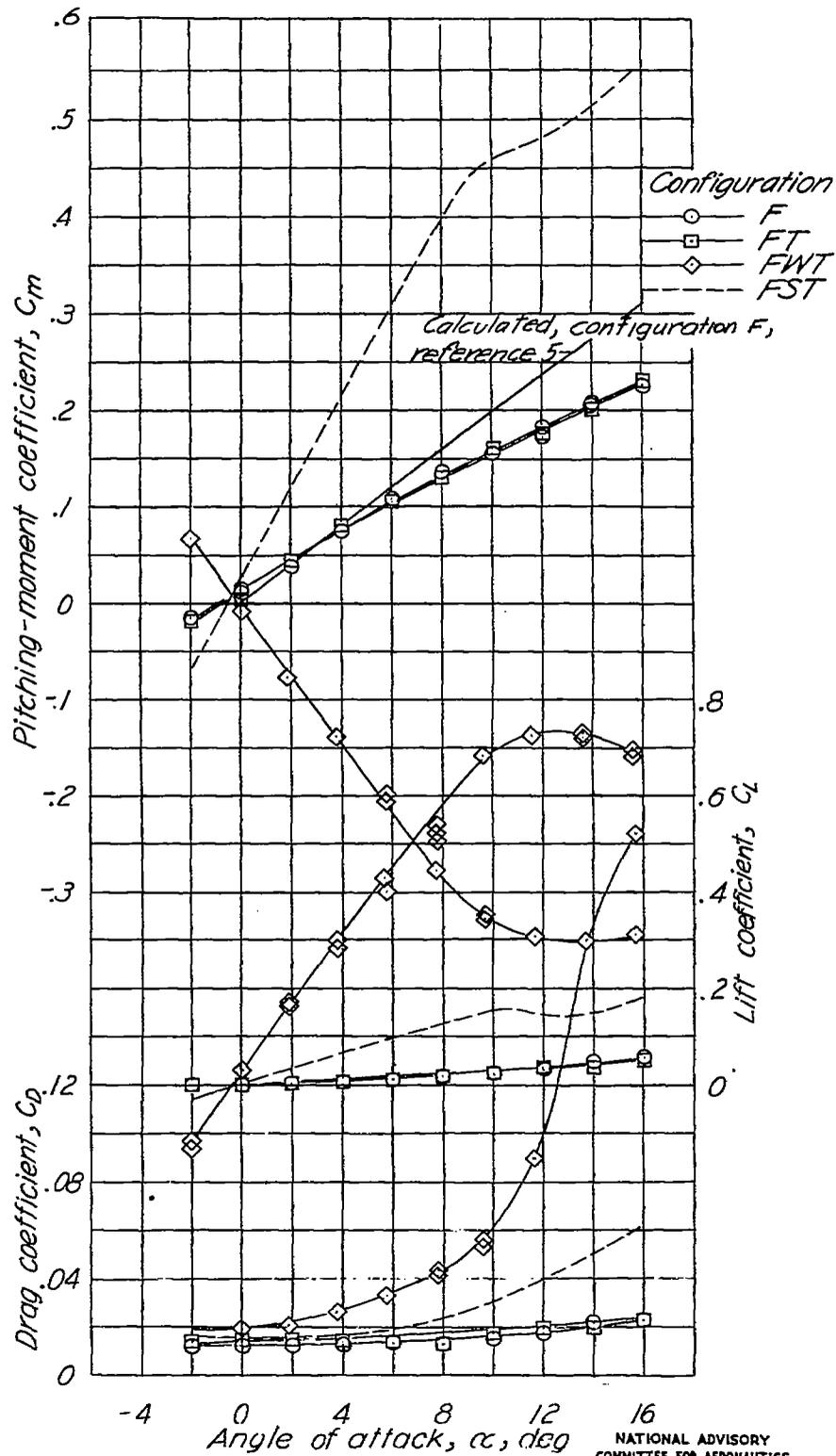
Figure 9 .- Variation of lift, drag, and pitching-moment coefficients with angle of attack for several configurations. $\psi=0°$.

Force measurements, FWT

$$\frac{C_L^2}{\pi A(.75)} + C_{D_0} = 0.070 \, C_L^2 + C_{D_0}$$

Induced drag coefficient computed from measured span-wise loading: $\frac{C_L^2}{\pi A(.79)} = 0.066 \, C_L^2$

Minimum induced drag coefficient (reference 1):

$$\frac{C_L^2}{\pi A\left(1 - 2\left(\frac{d}{b}\right)^2 + \left(\frac{d}{b}\right)^4\right)} = \frac{C_L^2}{\pi A(.97)} = 0.054 \, C_L^2$$

C_D

C_L^2

NATIONAL ADVISORY
COMMITTEE FOR AERONAUTICS

(a) Configuration FWT.

Figure 10.— Variation of drag coefficient with square of lift coefficient.

Force measurements, FST

Induced drag coefficient computed from measured span-wise loading:

$$\frac{C_{L_S}^2}{\pi A(.81)} = 0.074 C_{L_S}^2$$

Minimum induced drag coefficient (reference 1):

$$\frac{C_{L_S}^2}{\pi A\left(1-2\left(\frac{d_S}{b_S}\right)^2 + \left(\frac{d_S}{b_S}\right)^4\right)} = 0.074 C_{L_S}^2$$

C_{D_S}

$C_{L_S}^2$

NATIONAL ADVISORY
COMMITTEE FOR AERONAUTICS
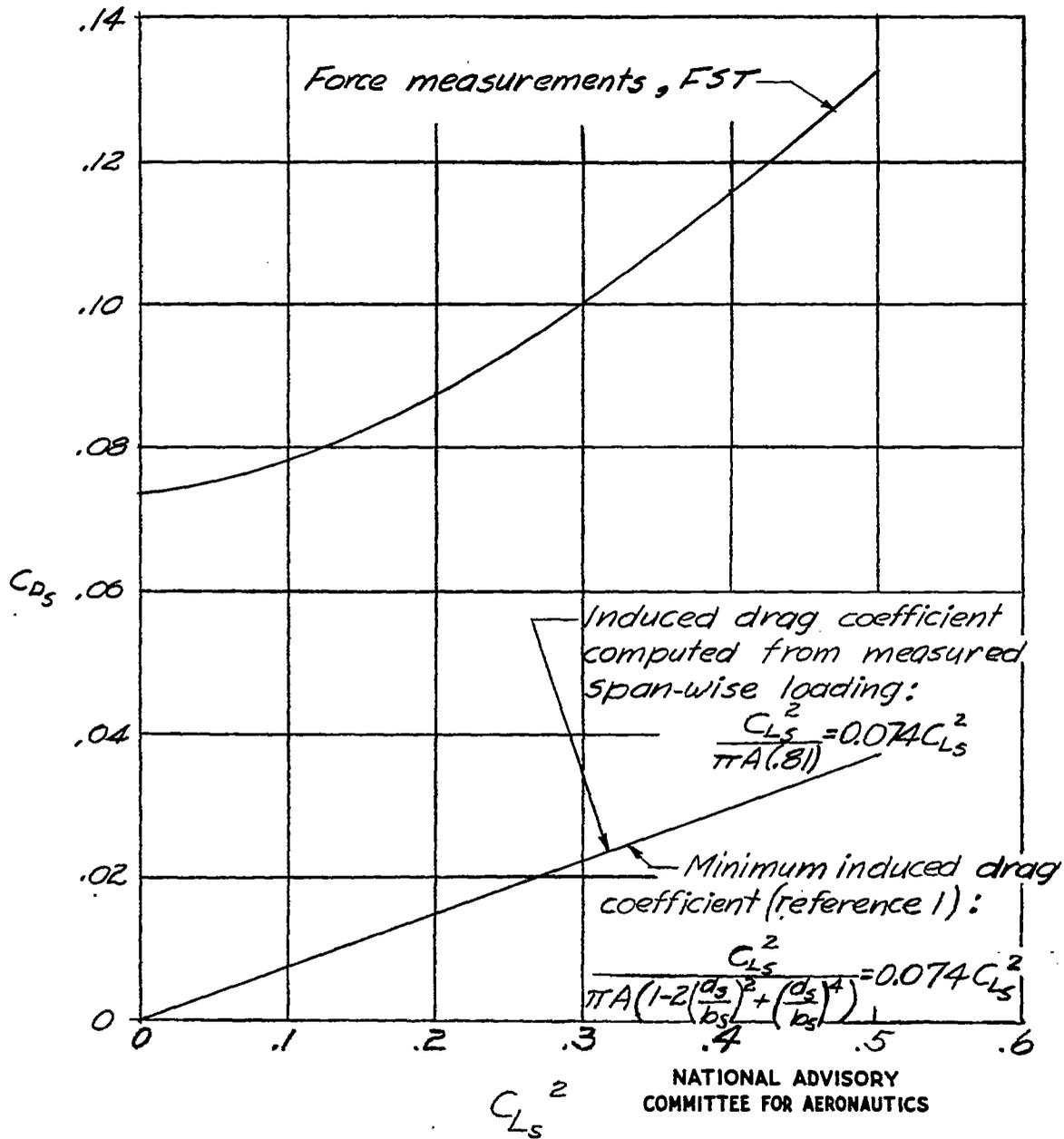
(b) Configuration FST.

Figure 10.— Concluded.